REST Journal on Emerging trends in Modelling and Manufacturing
Vol:4(1),2018
REST Publisher
ISSN: 2455-4537

Website: www.restpublisher.com/journals/jemm

Synthesis, characterisation and evaluation of photocatalytic activity of V-doped SnO_2 semiconducting particles under solar light

R. Shyamala and L. Gomathi Devi*
Department of Post-Graduate Studies in Chemistry, Central College City Campus,
Dr. Ambedkar Street, Bangalore University, Bangalore-560001
Email: shyamala.r98@gmail.com **and** *gomatidevi_naik@yahoo.co.in*

Abstract

The vanadium doped tin(iv)oxide (V/SnO_2) was synthesized via sol gel method using ammonium metavanadate and stannous chloride dihydrate and the concentration of the vanadium was varied from 2 at.% to 10 at.% and the samples were designated as 2 at.%-V/SnO_2, 4 at.%-V/SnO_2, 6 at.%-V/SnO_2 and 10 at.%-V/SnO_2. The catalysts were characterized by PXRD, UV-vis absorbance and FTIR. The phase purity, lattice constant values, crystallite size, cell volume and lattice strain values were obtained from PXRD technique. A UV-vis absorbance spectrum shows the variation of band gap from 3.7-2.9 eV for the above mentioned samples. An FTIR study shows the V_2O_5 vibrational modes at 850 cm^{-1} and 967 cm^{-1}. Enhanced photocatalytic activity of 6 at.%-V/SnO_2 under solar light was accounted to the efficient charge carrier separation of photogenerated electron-hole pairs and also to its dopant energy level facilitating charge carrier migration.

Key words: Semiconductor; Photocatalysis; Vanadium; Tin (IV) oxide; trapping sites and electron hole recombination.

1. Introduction

An intense research has been devoted in recent years to lower the threshold excitation energy of the semiconducting nano materials in order to utilize large fraction of solar light with high efficiency. In this regard, metal oxides such as TiO_2, SnO_2 and ZnO were found to be very useful in developing catalysis mainly for the control of environmental pollution. Tin oxide (SnO_2) nanostructures are widely applied in various fields. It is well known that chemisorbed active oxygen species on SnO_2 surface can affect the electronic and catalytic properties of the host material (*1*). More specifically pure SnO_2 may not be a good oxidation catalyst due to its low activity and wide band gap (~3.4-3.8 eV) (*2*). To suppress the photogenerated electron–hole recombination and to reduce its band gap one of the approach is to dope the SnO_2 with other suitable transition metal ions. The mid band gaps created due to the doping may extend its photoresponse to visible region of the solar spectrum (*3*). The doping of semiconducting oxides with transition metal ions has attracted significant interest over the years, since even low levels of bulk dopants can have a major impact on the electronic properties of these materials (*4-11*). Among the transition metal ions, vanadium ion is attractive because it can increase photogenerated charge carrier lifetime and apparently it can also extend the absorption range of SnO_2 (12, *13*). Depending on the oxidation state of V, the position of donor levels and electronic properties can be altered. Specifically, vanadium can be easily doped into SnO_2 as its ionic radius (V^{5+}/Sn^{4+} = 0.59/0.69 A˚) is smaller than the host Sn^{4+} ion. Both SnO_2 and V_2O_5 are amphoteric in nature. Catalytic activity of V doped SnO_2 is expected to show higher activity due to its ability to lose or gain oxygen. Therefore, doping of vanadium in to the SnO_2 lattice is attempted in the present research and the aim is to study the physicochemical properties of the material which facilitates the catalytic efficiency in a photochemical reaction.

2. Results

2.1. PXRD analysis

Fig.1 shows the PXRD patterns of the SnO_2 and V/SnO_2 samples. The diffraction patterns of SnO_2 and V/SnO_2 samples were indexed to the tetragonal rutile structure of SnO_2 (JCPDS 41-1445) (*14*, *15*). The ionic radius of V^{5+} = 0.59 A˚ is smaller than the Sn^{4+} (0.69 A˚) ion. Hence, V^{5+} ion can easily substitute Sn^{4+} ion in SnO_2 lattice without distorting the phase structure of SnO_2 and therefore the PXRD patterns of V/SnO_2 does not change. The average crystallite size (D) was calculated in accordance with Scherer's formula using full width at half maximum (FWHM) data.

$$D = \frac{K\lambda}{\beta\cos\theta} \quad (1)$$

Where, K is the shape factor which is a constant (~ 0.9), λ is the X-ray wavelength (0.15418 nm), β is the full width at half maximum (FWHM) of the diffraction peak and θ is the angle of diffraction. The values of β and θ are taken for the (100) crystal plane of rutile phase. The crystallite sizes were found to be 10.94, 12.35, 16.69, 21.96, and 10.96 nm for SnO_2 and for V/SnO_2 with dopant concentrations of 2 at.%, 4 at.%, 6 at.% and 10 at.%, respectively (Table S1.). These results suggest that the incorporation of V^{5+} ion into the SnO_2 lattice is effectively facilitating the rutile grain growth. A new peak is observed around 32˚ due to the formation of V_2O_5 when concentration was higher 10 at% and the crystallite size for this sample

decreases. This may be because at higher dopant concentration, the dopant ions instead of occupying substitutional lattice positions, they may occupy the interstitial positions in the SnO_2 lattice decreasing the crystallite size (*16*).
The X-ray diffraction peaks pertaining to (100), (101) and (200) crystal planes of rutile were selected to determine the values of lattice parameters of SnO_2 and V/SnO_2 samples by using the following equations:

$$d = \frac{n\lambda}{2\sin\theta} \quad (2)$$

$$\frac{1}{d^2} = \frac{h^2}{a^2} + \frac{k^2}{b^2} + \frac{l^2}{c^2} \quad (3)$$

Where d is the distance between crystal planes of (h k l), λ is the X-ray wavelength, θ is the diffraction angle and a, b, c are the lattice parameters. The calculated values of crystallite size, lattice parameters, cell volume and lattice strain for SnO_2 and V/SnO_2 samples are given in Table S1. The crystallite size keeps increasing with dopant concentration up to the dispersion capacity. An incremental increase in the length of the c-axis takes place with increase in the dopant concentration. Doping of V^{5+} ion in to the SnO_2 lattice appears to follow Vegard's law (*17*). The volume of the unit cell decrease as the V content increases. Such lattice contraction can be due to the smaller size of the dopant ion and also its local coordination.

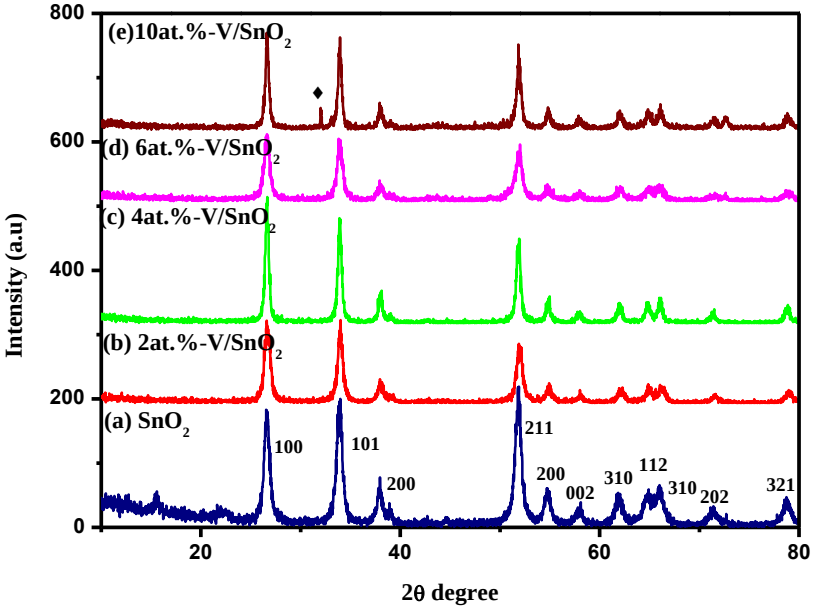

Fig.1. The PXRD patterns of: (a) SnO_2, (b) 2 at.%-V/SnO_2, (c) 4 at.%-V/SnO_2, (d) 6 at.%-V/SnO_2 and (e) 10 at.%-V/SnO_2 catalysts.

2.2. UV-visible absorbance spectroscopic analysis

Fig.2 displays UV–vis absorbance spectra of the SnO_2 and V/SnO_2 samples. The extended absorption in the visible region can be attributed to the charge transfer from oxygen 2p levels of valence band (VB) to the t_{2g} level of vanadium, which lies just below the conduction band (CB) of SnO_2. As the V dopant content increases (i.e., V/SnO_2 from 2 to 10 at.%), the absorption spectrum broadens remarkably and extends in to the visible region which is associated with the $O^{2-} \rightarrow V^{5+}$ charge transfer in an octahedral environment (4). The absorption edge shows a red-shift with increase in dopant concentration due to the formation of V–O–V bonds (*18*). The position of dopant electronic energy level change with dopant concentration and hence the indirect band gap values of the doped samples also change. The band gap energies of the catalysts were calculated by the Planck's equation, Eqn. (4).

$$E_g = \frac{hc}{\lambda} = \frac{1240}{\lambda} \quad (4)$$

Where E_g is the band gap of the sample (eV) and λ is the wavelength corresponding to the absorption edge (nm) obtained from the intersection point on the wavelength axis from the tangents drawn to the absorption curve. Absorption coefficient (α) values of SnO_2 and V/SnO_2 samples were calculated from the Eqn. (5).

$$\alpha = \frac{4\pi k}{\lambda} \quad (5)$$

Where k is the absorption index or absorbance value for the wavelength (λ) corresponding to the bandgap, since the majority of the electronic transition in the lattice takes place from VB to the CB. The absorption coefficient value decreases for 2 at.%-V/SnO_2 and 4 at.%-V/SnO_2 samples. But α value increases for 6 at.%-V/SnO_2 sample and again decreases for 10 at.%-V/SnO_2 sample. The band gap 'E_g' values and the 'α' values are given in Table. S2.

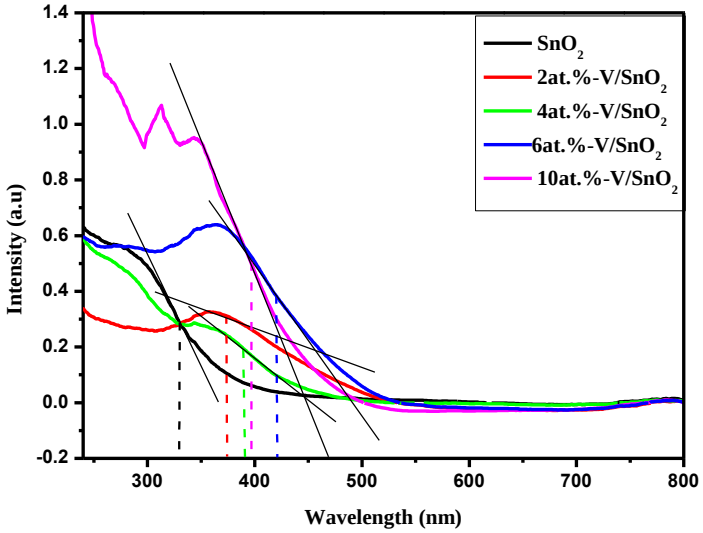

Fig.2. The absorbance spectra of the SnO_2 and V/SnO_2 catalysts.

2.3. FTIR analysis

FTIR spectra of SnO_2 and V/SnO_2 samples are shown in Fig.3A. The Sn-O stretching vibrations are found in the region of 800-300 cm^{-1} (*19*). The peak observed at 604 cm^{-1} is assigned to Sn-O-Sn stretching vibrations and the band obtained at 473 cm^{-1} is attributed to terminal Sn-O vibration of Sn-OH group. Many simple metal oxides with more than one oxygen atom bound to a single metal atom usually absorb in the IR region of 1020–970 cm^{-1} and a peak at 967 cm^{-1} can be assigned to V_2O_5 vibrational modes. In the present study the peak observed at 850 cm^{-1} can be due to V-O-V stretching vibrations (*20, 21*). Fig.3B shows the vanadium bridging vibrations. The broad band at around 1258 cm^{-1} can be attributed to the bending vibrations of terminal Sn-OH groups. A peak observed at 1643 cm^{-1} is attributed to the bending vibration of adsorbed water molecules. A broad band was observed at 3386 cm^{-1} indicates the presence of hydrogen bonded -OH group on the surface of SnO_2 particles.

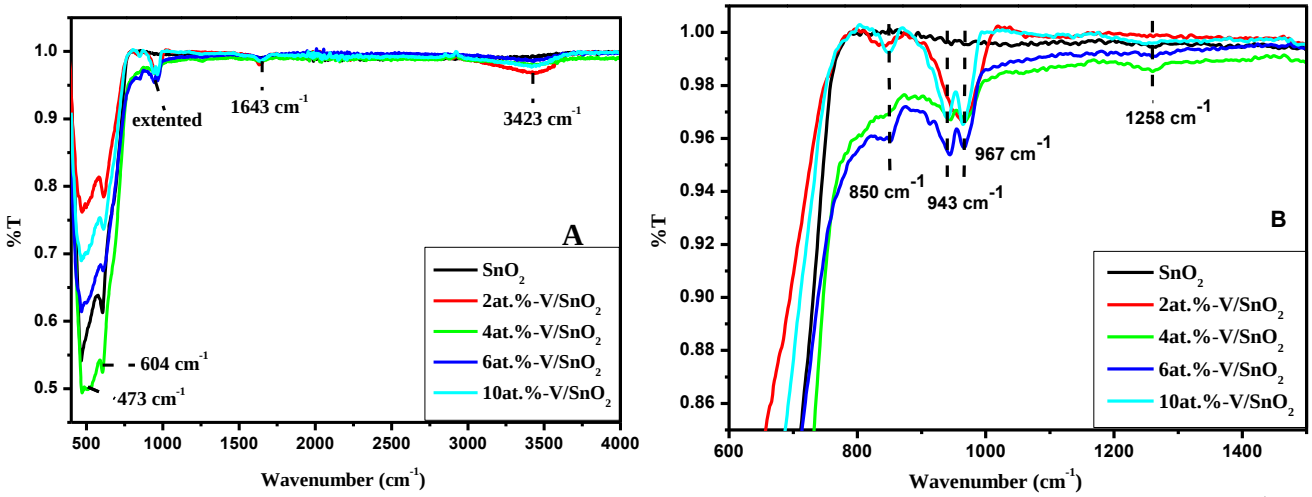

Fig.3. (A) FTIR spectra of the SnO_2 and V/SnO_2 samples. (B) FTIR spectra magnified in the region of 600 to 1400 cm^{-1}.

2.4. SEM analysis

The surface morphology of SnO_2 and 6at.%-V/SnO_2 was obtained by the SEM technique and are shown in Fig.4A and B respectively. No characteristic morphology was observed for both the samples. The calculation of particles size distribution was done by using image j software for all the samples. The average particle size of SnO_2 was found to be 4.57 µm and the area under the curve is found to be A=61.01. Whereas the average particles size of 6at.%-V/SnO_2 particles was found to be 18.65 µm and the area under the curve is A= 1353.87. EDAX analysis for SnO_2 and 6at.%-V/SnO_2 are shown in Fig. 4C and D. The results confirm the presence of O and Sn in SnO_2 (Fig.4C) and V, O and Sn in 6at.%-V/SnO_2 sample (Fig.4D).

(A)

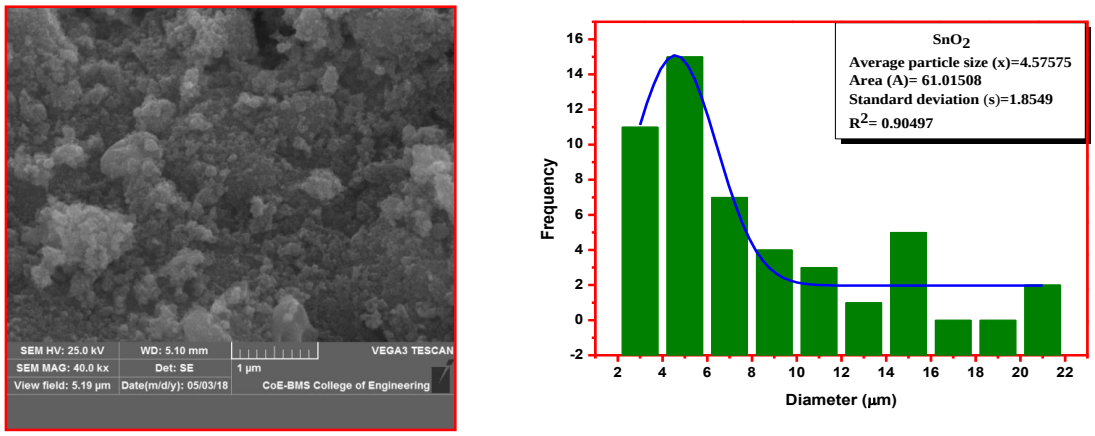

(B)

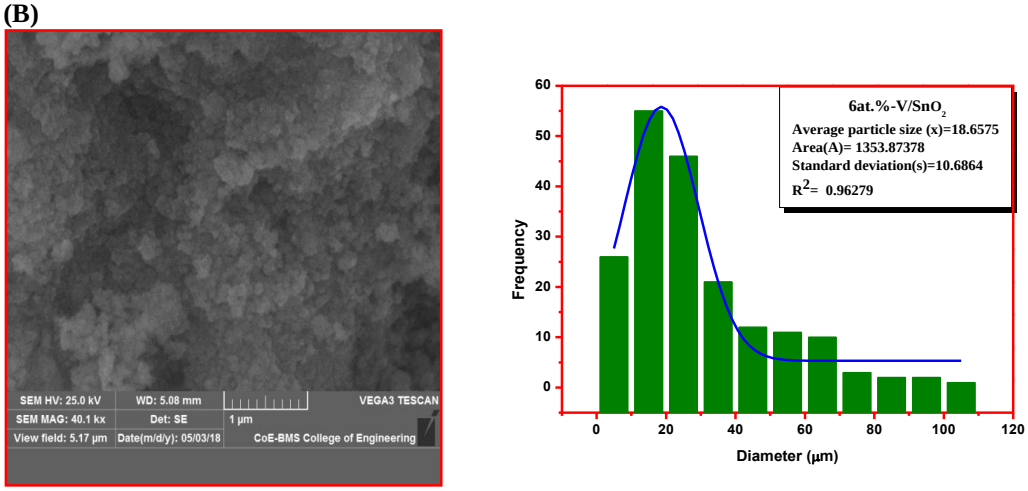

(C)

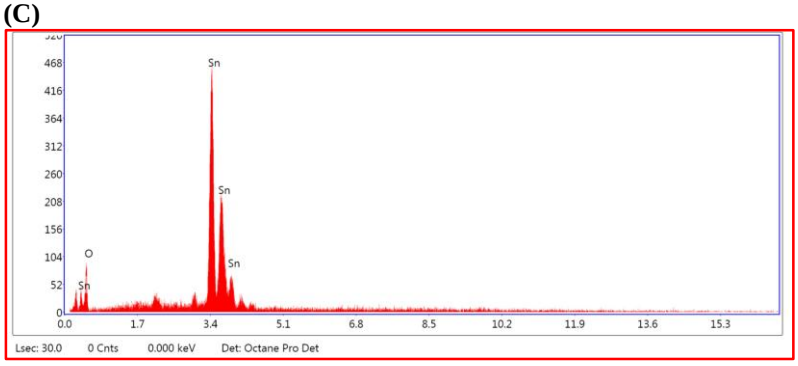

(D)

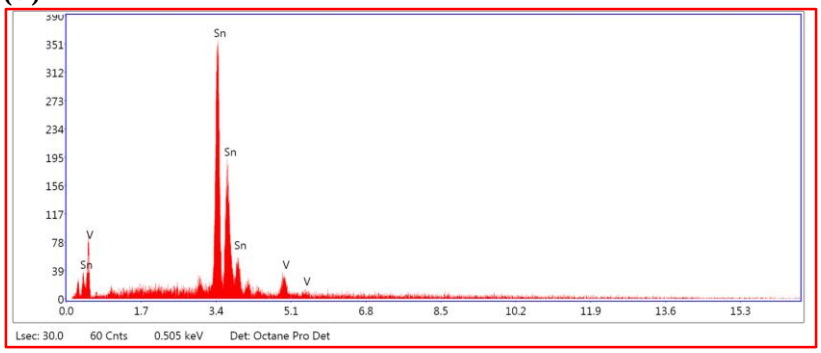

Fig.4. SEM images and the particle size distribution curves for (A) SnO_2, (B) 6at.%-V/SnO_2 catalyst and EDAX of (C) SnO_2, (D) 6at.%-V/SnO_2 photocatalysts.

2.5. Photocatalysis analysis

The photocatalytic activities of SnO_2 and V/SnO_2 samples were evaluated by taking MO (10 ppm) as the model pollutant compound in 250ml of aqueous solution under the solar irradiation. From the results it can be inferred that the photocatalytic activity of the V doped samples are higher compared to the SnO_2 sample and the order of the photodegradation reactivity of

the samples are MO < SnO_2 < 2at.%-V/SnO_2 < 4at.%-V/SnO_2 < 10at.%-V/SnO_2 < 6at.%-V/SnO_2 (Fig.5A). 6at.%-V/SnO_2 shows higher activity compared to all the other samples. The absorbance spectra was recorded at different time intervals for the degradation reaction with 6at.%-V/SnO_2 sample (Fig.5B). The values of % degradation were directly taken from the curves given in the Fig.5A. The degradation reaction was found to follow first order kinetics. The rate constant values were obtained from negative slope of the straight lines from the plot of log C/C_0 verses time. The degradation of aqueous organic pollutant in a light induced process represents a major fraction of operating costs. A simplified equation for evaluating electric energy consumption (as light energy) and the same is adopted in this research study (*22*, *23*). EE_O is defined as the number of KWh of electrical energy required to reduce the concentration of pollutant by one order of magnitude 1 m^3 of contaminated water. EE_O can be calculated using the following Eqn (*24*):

$$EE_O = \frac{38.4 \times P}{V \times k} \qquad (6)$$

Where P (0.125) is the power of the light source in KW, V (250) is the volume of the reaction solution in ml and k is the rate constant (min^{-1}) for the degradation of the MO. EE_O is expressed in terms of $KWhm^{-3}$ $order^{-1}$ and the results for all the SnO_2 and V/SnO_2 catalysts are given in Table.1

The following reaction mechanism can occur at dopant levels

$$V^{5+} + e^- \rightarrow V^{4+} \qquad (7)$$

$$V^{4+} + O_2(\text{adsorption}) \rightarrow V^{5+} + O_2^{\bullet-} \qquad (8)$$

$$V^{5+} + h^+ \rightarrow V^{6+} \qquad (9)$$

$$V^{6+} + OH^- \rightarrow V^{5+} + OH^{\bullet} \qquad (10)$$

Trapping and detrapping of the charge carrier showed by the V doped SnO_2 photocatalyst can be accounted to its electronic configuration. V^{5+} posses completely empty'd' and's' orbital's which are highly stable. When the V traps the electron or holes this stability is disturbed and the dopant attains the stable state by detrapping it. This kind of trapping is referred to as shallow trapping. The trapping and detrapping accelerates interfacial charge transfer process leading to the excess generation of super oxide and hydroxyl radicals. Therefore it can be concluded that the prerequisite condition for the dopant to be effective lies in its optimum concentration which facilitate the formation of appropriate dopant energy levels and surface states for the smooth migration of charge carriers (Fig.6).

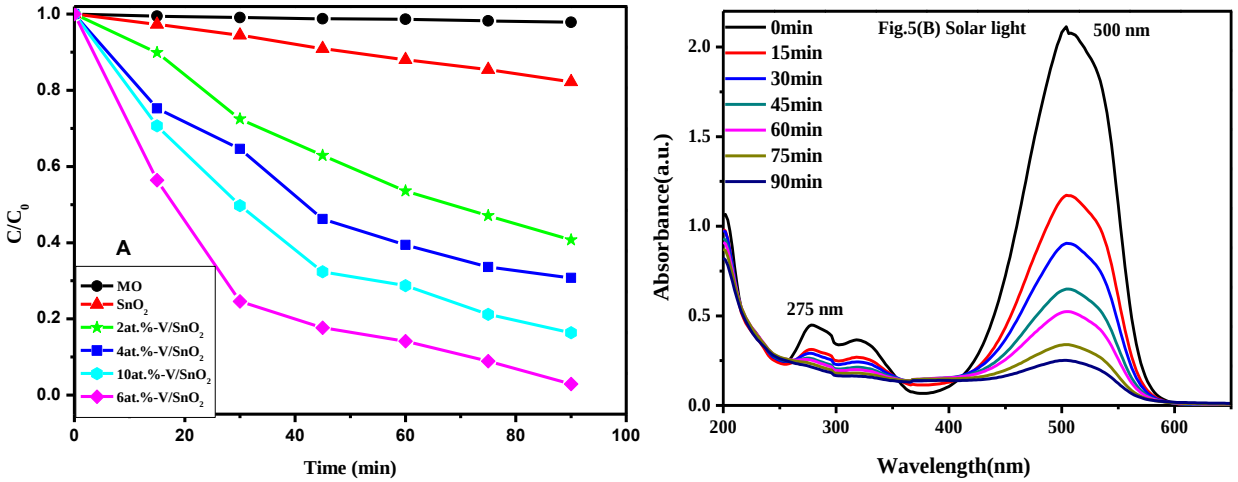

Fig.5. (A) The plot of C/C_0 verses time (min) of the undoped SnO_2 and V/SnO_2 catalysts.
(B) UV-visible absorbance spectra recorded at different time intervals for the degradation reaction of MO using 6at.%-V/SnO_2 photocatalyst.

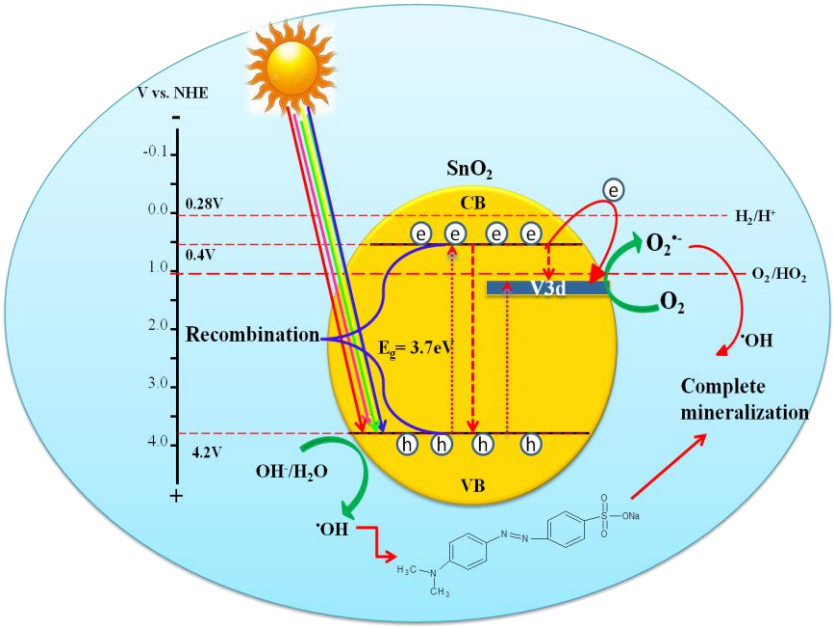

Fig.6. The possible pictorial representation of the absorption of energy and the electron transfer reaction on the V/SnO_2 catalysts.

Table.1. The values of % degradation, rate constant (k) and electrical energy per order (EE_O) for the various experiments as mentioned under solar light irradiation.

catalyst	**% degradation (solar-light)**	**Rate (k)x10^{-2}** min^{-1}	**EE_O** $KWhm^{-3}$ order-1
MO in the absence of catalyst	2.1	0.022	87.27
SnO_2	17	0.219	8.76
2at.%-V/SnO_2	59.3	1.022	1.87
4at.%-V/SnO_2	69.2	1.345	1.42
6at.%-V/SnO_2	98.1	3.543	0.54
10at.%-V/SnO_2	83.6	1.997	0.96

3. Conclusion

SnO_2 and V/SnO_2 catalysts were prepared by sol gel method and characterized by XRD, FTIR, SEM, EDAX and absorbance UV–visible spectroscopy. V/SnO_2 samples showed a tetragonal rutile structure similar to that of undoped SnO_2 with no trace of any other crystalline oxide phase below the optimum dopant concentration. FTIR and EDAX study confirms the incorporation of V in to the SnO_2 lattice. The band gap of V/SnO_2 samples decreases from 3.77 to 2.9 eV as the V concentration increased from 2 to 10 at%. The photocatalytic activities of the SnO_2 and V/SnO_2 catalysts were determined by studying the photodegradation of MO as a model organic pollutant. The highest photocatalytic activity was obtained with the 6at.%-V/SnO_2 sample due to lower band gap value and higher absorption coefficient. It can be concluded that the prerequisite condition for the dopant to be effective lies in its optimum concentration which facilitate the formation of appropriate dopant energy levels and surface states for the smooth migration of charge carriers.

Experimental Design

Materials

Stannous chloride dihydrate ($SnCl_2.2H_2O$), Ethylene glycol (EG), Sodium acetate tri-hydrate ($CH_3COONa.3H_2O$), Ammonium metavanadate (NH_4VO_3) were brought from Aldrich and methyl orange (MO) was obtained from SD fine chemicals.

Preparation of SnO_2 and V/SnO_2

4.23 g of $SnCl_2.2H_2O$ was dissolved in 50 mL of EG and 5.1g of $CH_3COONa.3H_2O$ was dissolved in 50 mL EG separately. A calculated amount of NH_4VO_3 is also dissolved in 25 mL of EG. $SnCl_2.2H_2O$ solution was taken in a three necked flask and appropriate volume of demineralised water was added to adjust the hydrolysis ratio and to obtain the pH 7. The other two solutions were added drop wise slowly with continues stirring. The resulting solution was heated at 160 ˚C for 7h. The white precipitate obtained was isolated by centrifugation and then calcined at 600 ˚C for 8h to yield V/SnO_2 samples. The concentration of V was varied as 2at.% (0.041 g), 4at.% (0.123 g), 6at.% (0.164 g) and 10at.% (0.411 g) to prepare samples with different dopant concentrations. The resulting samples are designated as 2at.%-V/SnO_2, 4.at%-V/SnO_2, 6.at%-V/$SnO_2$and 10at.%-V/SnO_2. SnO_2 sample was also prepared by the similar method and in this case the solution containing V was avoided.

Acknowledgements

Authors acknowledge to the Bangalore University of Bangalore for financial and other supports and also many thanks for Government of India and Other Backward Cell (OBC) Bangalore, for their financial supports.

Conflict of interest: there is no conflict of interest.

References

[1]. T. Kawabe, K. Tabata, E. Suzuki, Y. Nagasawa. "Methanol adsorption on SnO_2 thin films with different morphologies." *surface science*, 482–485 (2001):183-188.

[2]. Chien-Tsung Wang, De-Lun Lai, Miao-Ting Chen. "Surface and catalytic properties of doped tin oxide nanoparticles."*Applied Surface Science*, 257 (2010):127–131.

[3]. Maruska HP, Ghosh AK. "A study of Oxide-based heterostructure photo electrodes" *Solar Energy Materials*, 1 (1979): 411-429.

[4]. K. Anandan, V. Rajendran. "Influence of dopant concentrations (Mn = 1, 2 and 3 mol %) on the structural, magnetic and optical properties and photocatalytic activities of SnO_2 nanoparticles synthesized via the simple precipitation process." *Superlattices and Microstructures*, 85 (2015):185–197.

[5]. Zhenfei Tian, Changhao Liang, Jun Liu, Hemin Zhang and Lide Zhang. "Zinc stannate nanocubes and nanourchins with high photocatalytic activity for methyl orange and 2, 5 -DCP degradation." *Journal of Materials Chemistry*, 22 (2012):17210-17214.

[6]. Jun Seop Lee, Oh Seok Kwon and Jyongsik Jang. "Facile synthesis of SnO_2 nanofibers decorated with N-doped ZnO nanonodules for visible light photocatalysts using single-nozzle co-electrospinning." *Journal of Materials Chemistry*, 22 (2012):14565-14572.

[7]. J.J. Murciaa, M.C. Hidalgo, J.A. Navío, J. Arana, J.M. Dona-Rodríguez. "Study of the phenol photocatalytic degradation over TiO_2 modified by sulfation, fluorination, and platinum nanoparticles photodeposition." *Applied Catalysis B: Environmental*, 179 (2015):305–312.

[8]. Shendong Zhuang, Xiaoyong Xu, Bing Feng, Jingguo Hu, Yaru Pang, Gang Zhou, Ling Tong, and Yuxue Zhou. "Photogenerated Carriers Transfer in Dye−Graphene−SnO_2 Composites for Highly Efficient Visible-Light Photocatalysis" *ACS Applied Material and Interfaces*, 6 (2014):613−621.

[9]. Quanjun Xiang, Jiaguo Yu and Mietek Jaroniec. "Graphene-based semiconductor photocatalysts" *Chemical society review*, 41 (2012):782-796.

[10]. H.R. Pouretedala, Z. Tofangsazi, M.H. Keshavarz. "Photocatalytic activity of mixture of ZrO_2/SnO_2, ZrO_2/CeO_2 and SnO_2/CeO_2 nanoparticles."Journal of Alloys and Compounds, 513, (2012), 359– 364.

[11]. L. Gomathi Devi, M.L. ArunaKumari , B.G. Anitha , R. Shyamala , G. Poornima. "Photocatalytic evaluation of Hemin (chloro(protoporhyinato)iron(III)) anchored ZnO hetero-aggregate system under UV/solar light irradiation: A surface modification method." *Surfaces and Interfaces*, 1–3 (2016):52–58.

[12]. Chien-Tsung Wang, De-Lun Lai, Miao-Ting Chen. "Surface and catalytic properties of doped tin oxide nanoparticles" *Applied Surface Science*, 257 (2010):127–131.

[13]. M. Gratzel, R.F. Howe. "Electron Paramagnetic Resonance Studies of Doped TiO_2, Colloids" *Journal of Physical Chemistry*, 94 (1990):2566.

[14]. Yinghuan Fu, Hongchao Ma, Zhenl¨u Wang, Wanchun Zhu, Tonghao Wu, Guo-jia Wang. "Characterization and reactivity of SnO_2-doped V_2O_5/γ-Al_2O_3 catalysts in dehydrogenation of isobutane to isobutene." *Journal of Molecular Catalysis A: Chemical*, 221 (2004):163–168.

[15]. L. Gomathi Devi and R. Photocatalytic activity of SnO_2–a-Fe_2O_3 composite mixtures: exploration of number of active sites, turnover number and turnover frequency." *Material Chemistry Frontiers*, 2 (2018):796

[16]. M. Jayalakshmi, M. Mohan Rao, N. Venugopal, Kwang-Bum Kim. "Hydrothermal synthesis of SnO_2-V_2O_5 mixed oxide and electrochemical screening of carbon nano tubes (CNT), V_2O_5, V_2O_5-CNT, and SnO_2-V_2O_5-CNT electrodes for supercapacitor applications." *Journal of Power Sources*, 166 (2007):578–583

[17]. L. Gomathi Devi, B. Narasimha Murhty, S. Girish Kumar Liu Jianhua. "Photo Catalytic Degradation of Imidachloprid Under Solar Light Using Metal Ion Doped TiO_2 Nano Particles: Influence of Oxidation State and Electronic Configuration of Dopants." *Cataylitic Letters*, 130 (2009):496–503.

[18]. Liu Jianhua, Yang Rong, Li Songmei. "Synthesis and Photocatalytic Activity of TiO_2 /V_2O_5 Composite Catalyst Doped with Rare Earth Ions." *Journal of rare Earths*, 25 (2007):173 – 178.

[19]. V. Baranauskas, M. Fontana, Z.J. Guo, H.J. Ceragioli, A.C. Peterlevitz. "Field-emission properties of nanocrystalline tin oxide films." *Sensors and Actuators B*, 107 (2005):474-478.

[20]. B. Bootz, H. Finkenrath, G. Franz, N. Uhle. "Long-Wave optical vibrations of V_2O_5" *Solid State Communications*, 13 (1973):1477.

[21]. F.J. Anaissi, G.J.-F. Demets, H.E. Toma, S. Dovidauskas, A.C.V. Coelho. "Characterization and properties of mixed bentonite-vanadium (V) oxide xerogels." *Materials Research Bulletin*, 36 (2001):289–306.

[22]. J.R. Bolton, K.G. Bircger, W. Tumas, C.A. Tolman. "Figures-of-merit for the technical development and application of advanced oxidation technologies for both electric- and solar-driven systems." *Pure and Applied Chemistry*, 73 (2001):627-637

[23]. N. Daneshvar, A. Aleboyeh, A.R. Khataee. "The evaluation of electrical energy per order (EEo) for photooxidative decolorization of four textile dye solutions by the kinetic mode." *Chemosphere*, 59 (2005) 761-767.

[24]. L. Gomathi Devi, B. G. Anitha. "Exploration of vectorial charge transfer mechanism in TiO_2/$SrTiO_3$ composite under UV light illumination for the degradation of 4-Nitrophenol: A comparative study with TiO_2 and $SrTiO_3$." *Surfaces and Interfaces*, 11 (2018):48-56.

Supplementary data

Table S1. Average crystallite size (D), lattice parameters (a = b, c), cell volume (V) and lattice strain (ε) values of SnO_2 and V/SnO_2 photocatalysts.

Photocatalyst	Crystallite size (nm)'D'	Lattice parameters (A˚)	Cell volume (A˚)^3'V'	Lattice strain (x10^{-3}) 'ε'
SnO_2	10.9434	a=b=4.736; c= 3.193	71.6181	13.76
2at.%-V/SnO_2	12.3556	a=b=4.747; c= 3.201	72.1314	12.2090
4at.%-V/SnO_2	16.6997	a=b=4.718; c= 3.191	71.0302	9.0165
6at.%-V/SnO_2	21.9682	a=b=4.752; c= 3.174	71.6737	6.8549
10at.%V/SnO_2	10.9606	a=b=4.738; c= 3.174	71.2519	13.7404

Table S2. Absorption coefficient (α) and Band gap (eV) values of SnO_2 and V/SnO_2 photocatalysts.

Photocatalyst	Absorption coefficient (α)x10^{-3}	Band gap (eV)
SnO_2	27.37	3.77
2at.%-V/SnO_2	12.07	3.32
4at.%-V/SnO_2	23.26	3.18
6at.%-V/SnO_2	34.82	2.9
10at.%-V/SnO_2	22.31	3.12